Available online at www.eccomasproceedia.org
Eccomas Proceedia COMPDYN (2023) 2296-2314

ECCOMAS
Proceedia

COMPDYN 2023
9th ECCOMAS Thematic Conference on
Computational Methods in Structural Dynamics and Earthquake Engineering
M. Papadrakakis, M. Fragiadakis (eds.)
Athens, Greece, 12-14 June 2023

SHEAR DEFICIENT RC BEAMS RETROFITTED WITH INORGANIC-MATRIX COMPOSITES

Dario De Domenico[1], **Natale Maugeri**[1], **Paolo Longo**[1], **Matteo Mazzeo**[1], **Giuseppe Ricciardi**[1], **Antonino Quattrocchi**[1], **Roberto Montanini**[1], **Luigi Calabrese**[1]

[1] Department of Engineering, University of Messina,
Contrada Di Dio, 98166, Sant'Agata, Messina, Italy
{dario.dedomenico, natale.maugeri, paolo.longo, matteo.mazzeo, giuseppe.ricciardi,
antonino.quattrocchi, roberto.montanini, luigi.calabrese}@unime.it

Abstract

Reinforced concrete (RC) beams of existing framed buildings designed and realized 40-50 years ago are, in frequent cases, characterized by low amounts of transverse reinforcement and need rapid and efficient retrofitting interventions to meet the performance requirements of recent seismic standards. Externally bonded composites represent a popular technique that has the advantage (over concrete section enlargement and steel jackets) to keep the self-weight of the structure relatively unaltered. In this contribution, we present the results of an experimental campaign conducted at the University of Messina on shear deficient RC beams that are strengthened with U-wrapped externally bonded polyparaphenylene benzobisoxazole (PBO) Fabric Reinforced Cementitious Matrix (FRCM) systems applied through different configurations. Ten RC beams are tested up to collapse, including two control beams and eight beams retrofitted with PBO-FRCM systems. Different variables are included in the testing program, including the fiber orientation (90° and 45° with respect to the beam longitudinal axis), the number of layers (one and two), the steel stirrup spacing (200 and 300 mm), and the presence or not of the anchorage. The paper illustrates the main experimental results in terms of shear gain (in comparison to the control beams without FRCM), failure mode, deformation capacity, and fiber exploitation ratio. Additionally, numerical simulation of the tested beams is also performed through a 3D finite element model incorporating a fracture-plastic model for concrete and embedded truss elements with multilinear elastic-plastic material model for steel bars. The FRCM system is simulated via 3D solid elements for the matrix, combined with embedded truss elements for the fibers, the latter incorporating an analytical bond-slip law to numerically reproduce the fiber slippage at the fiber-matrix interface.

Keywords: Fabric-reinforced cementitious matrix (FRCM), Shear strengthening, Externally bonded FRCM, PBO-FRCM composites, RC beams, Numerical finite element model.

ISSN:2623-3347
Peer-review under responsibility of the organizing committee of COMPDYN 2023.
doi: 10.7712/120123.10561.21050

1 INTRODUCTION

Existing reinforced concrete (RC) framed buildings having more 50 years of service were realized with outdated design criteria and poor construction detailing, consequently they do not satisfy performance requirements of recent seismic standards. In Italy, one of the most frequent structural deficiencies is ascribed to the low shear capacity of RC beams, partly due to past design regulations [1]-[4]. As an example, minimum shear reinforcement of RC beams comprising 6 mm hoops spaced 25 cm combined with 45° inclined steel bars was suggested by the Royal Decree n. 2239 of 1939. This reinforcement amount represents, in most cases, not the minimum, but the actual transverse reinforcement observed in situ. Considering the brittle nature of shear failure and in view of capacity-design principles incorporated in modern performance-based standards [5]-[9], it is of utmost importance to increase the shear strength of existing RC beams through efficient, cost-effective, feasible, and rapid retrofit interventions. Within the broader class of composite materials, one of the most promising techniques to improve the shear capacity of existing RC beams consists of externally bonding Fabric Reinforced Cementitious Matrix (FRCM) systems to provide the desired supplemental shear reinforcement [10]-[13]. Apart from shear strengthening [14]-[16], this technique has proven to be effective also for increasing the confinement of reinforced concrete columns [17], [18], and for flexural strengthening [19]-[21]. Since in all such applications FRCM composites are externally bonded to the concrete substrate, the efficiency of this retrofitting technology strongly depends on the bond behavior at the FRCM-substrate interface [22]-[25] and the tensile properties of the composite in the uncracked, cracking and fully cracked phase involving the fabric-matrix interaction [26]-[29].

In this contribution, we present and critically interpret the results of an experimental campaign on full-scale (3.0 m long) RC beams that are designed to be shear deficient (two different shear reinforcement ratios ρ_w equal to 0.22% and 0.34% are considered) and over-reinforced in bending (longitudinal reinforcement ratio ρ_l equal to 5.66%). These beams are reinforced with U-wrapped externally bonded polyparaphenylene benzobisoxazole (PBO) sheets applied through different configurations, including one or two layers, fiber orientations at 90° and 45° with respect to the longitudinal axis of the beam, and presence or not of anchorage. All the beams are tested up to collapse under monotonic loading in four-point bending and failed in shear with a main diagonal crack. It has been observed that the increase of shear capacity over the control beams (without PBO sheets) is variable from 20% up to 40%, and the increase of deformation capacity (i.e., the displacement at peak load) ranges from 10% up to 65%. Electrical strain gauges are positioned on stirrups and fibers to monitor the strain response and to study the internal/external shear reinforcement interaction effects. Fiber exploitation ratios range from 10% to 35%, whereas the stirrups crossing the diagonal crack are largely yielded (with strains even five times higher than the yielding strain, depending on the strengthening configuration). Numerical simulation with a 3D finite element (FE) code is also performed to investigate some local mechanisms and to pave the way for a more systematic analysis of the internal-external shear reinforcement interaction through combined experimental and numerical approaches.

2 EXPERIMENTAL PROGRAM

A total of 10 RC beams are included in the experimental program. The beams have the same dimensions and steel reinforcement arrangement as those tested by Gonzalez-Libreros et al. [14] in 2017, with the exception of the top steel bars that are 2Ø20 in place of 2Ø16 (purposely changed to prevent premature concrete crushing phenomena at the compression zone,

near the loading regions, which was reported in the earlier experimental campaign). The beams have a width b = 150 mm, height h = 300 mm and total length L = 3000 mm.

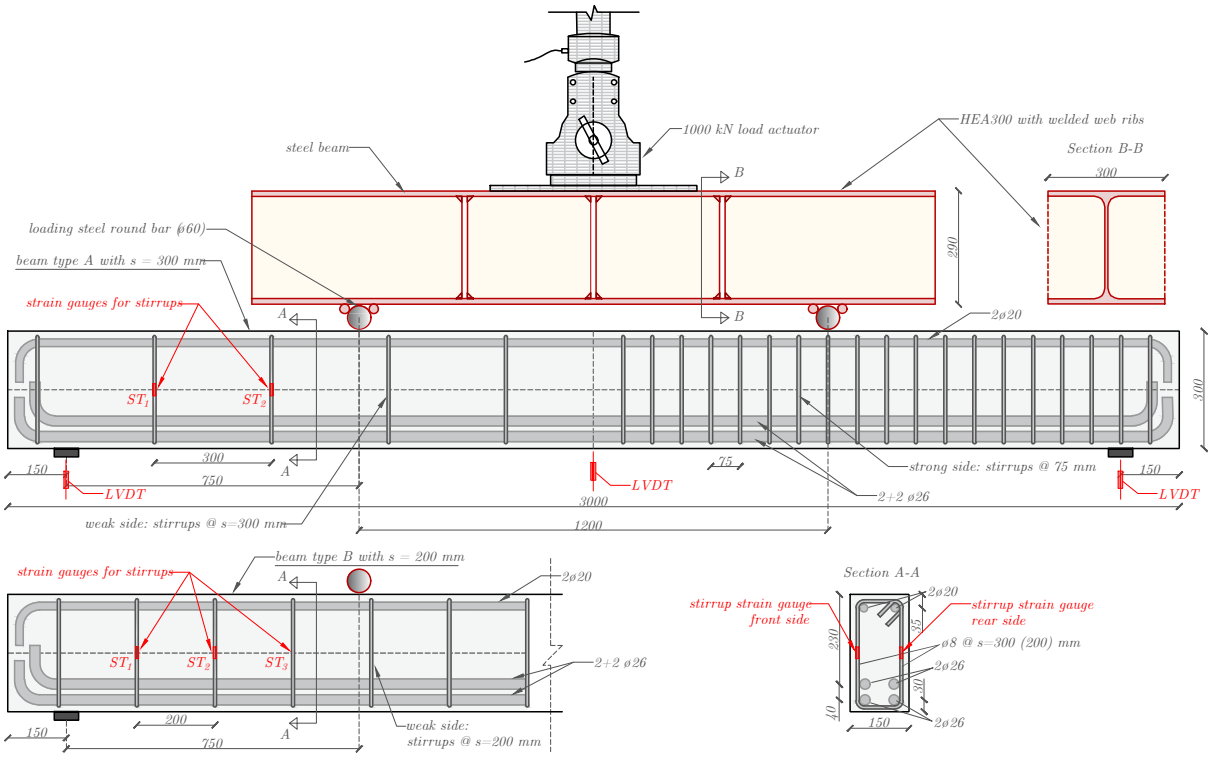

Figure 1: Test setup, instrumentation, and details of steel reinforcement (units in mm).

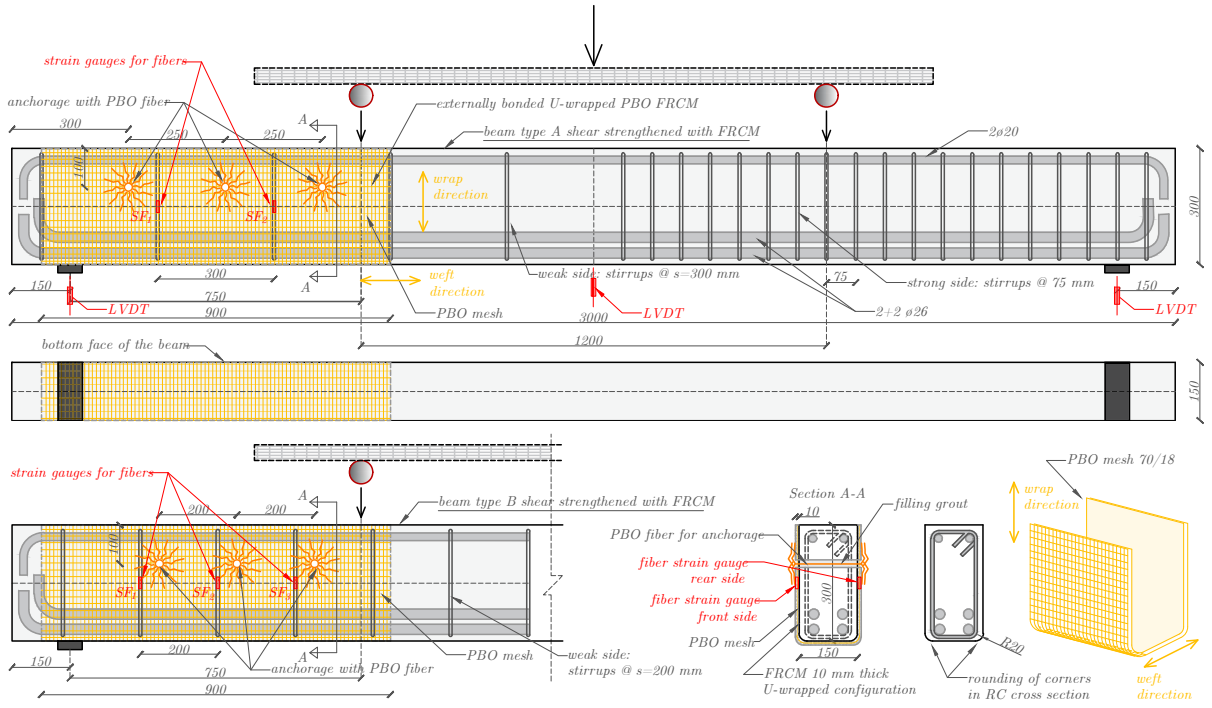

Figure 2: Strengthening configuration of tested beams (units in mm).

As shown in Figure 1, the beams are tested using a four-point bending scheme, with a span length l = 2700 mm and a shear span a = 750 mm (corresponding to a shear span-to-effective depth ratio a/d = 2.5, assuming a concrete cover 50 mm). The beams are over-reinforced in flexure and are weakly reinforced in shear with closed stirrups (two legs) spaced at 300 mm (beam type A) and 200 mm (beam type B) so as to trigger a shear-dominated failure mode. The transverse reinforcement is asymmetric along the beam length to study only one shear span (the left span as per the sketch in Figure 1); in the other span, stirrups are spaced 75 mm.

Eight out of the ten beams are shear strengthened (only in the weakly reinforced shear span, for a length equal to 900 mm) with a U-wrapped externally bonded PBO-FRCM system, as shown in Figure 2. Different number of layers (1 or 2) and fiber orientation angle (90° and 45° with respect to the longitudinal axis of the beam) are considered. The beams are designated with the following nomenclature: X-N-A-Y, where X denotes the type of beam (A or B, depending on the stirrups spacing in the studied shear span), N identifies the number of layers of PBO mesh (control, 1, or 2), A denotes the fiber inclination angle with respect to the beam longitudinal axis (90 and 45), and Y indicates the presence or not of the anchorage ("n" without anchorage, "a" with anchorage). The designation and strengthening characteristics of the tested beams (with corresponding nomenclature) are listed in Table 1.

Table 1: Designation and strengthening characteristics of the tested RC beams.

Series	Beam	s [mm]	PBO mesh angle	N. layers	Anchorage
A	A-control	200	-	-	-
	A-1-90-a	200	90°	1	Yes
	A-1-90-n	200	90°	1	No
	A-2-90-a	200	90°	2	Yes
	A-1-45-a	200	45°	1	Yes
B	B-control	300	-	-	-
	B-1-90-a	300	90°	1	Yes
	B-1-90-n	300	90°	1	No
	B-2-90-a	300	90°	2	Yes
	B-1-45-a	300	45°	1	Yes

Figure 3: Actual testing setup used in this experimental campaign.

2.1 Test procedure and instrumentation

The load P is applied to the tested beams through an actuator having 1000 kN load capacity. The actuator applies the load not to the concrete beam directly, but through an intermediate steel beam (HEA 300 with welded web ribs, as shown in Figure 1). The steel spreader beam is simply supported on the tested concrete beam and creates two symmetrical loading points (via two steel cylinders having 60 mm diameter), each placed at 600 mm from the beam mid-span. The beams are loaded up to failure in displacement-control mode, with a displacement rate 0.03 mm/s. Three linear variable displacement transducers (LVDTs), Solartron Metrology V10005SBN3 having stroke ±100mm, are placed below the beam to measure the mid-span deflection and near the support plates to check possible settlements at the support locations (including local crushing of the beam soffit). A photograph of the testing setup is reported in Figure 3.

Four and six strain gauges for the steel stirrups and an equal number of strain gauges for the fibers are placed in the beam type A and B, respectively (nomenclature $ST_{\#i}$ and $SF_{\#i}$). All electronic data are collected at a frequency of 10 Hz via a data acquisition system.

2.2 Materials

The steel reinforcement is prepared according to the design drawings reported in Figure 1; some phases of the preparation are illustrated in Figure 4. Deformed (ribbed) steel bars of grade B450C are used for both longitudinal and transverse reinforcement. Four Ø26 mm longitudinal bars are placed as bottom longitudinal reinforcement (A_{sl}), while two Ø20 mm steel bars are placed in the compression region. All longitudinal bars are anchored through 90° hooks at their ends. As said above, two-leg Ø8 mm closed stirrups are placed as transverse reinforcement (A_{sw}) with spacing 300 mm (beam type A) and 200 mm (beam type B) in the studied shear span.

Figure 4: Preparation of the steel reinforcement arrangement.

The yield strength of the bars is evaluated by means of tensile tests, in compliance wit EN ISO 6892-1 through a universal machine Quasar 1200; the measured yield strength f_{ym} of the Ø8 mm, Ø20 mm and Ø26 mm bars is 519 MPa, 518 MPa and 554 MPa, respectively. The

shear reinforcement ratio of the beams is $\rho_w = A_{sw}/b\ s$ = 0.22% and 0.34% for the beam type A and B, respectively, while the longitudinal reinforcement ratio $\rho_l = A_{sl}/b\ d$ = 5.66% (over-reinforced in bending).

The stirrups are instrumented with electrical strain gauges (SGs), with gauge length of 6 mm (120 Ω resistance), that are bonded in the mid-height of the steel bars (both sides, i.e., one SG for each leg) to monitor the steel strains in the tested shear span, as shown in Figure 5. As said above, four and six SGs for the beam type A and B are used, respectively, having nomenclature $ST_{i,front}$, $ST_{i,rear}$ as depicted in the sketch of Figure 1.

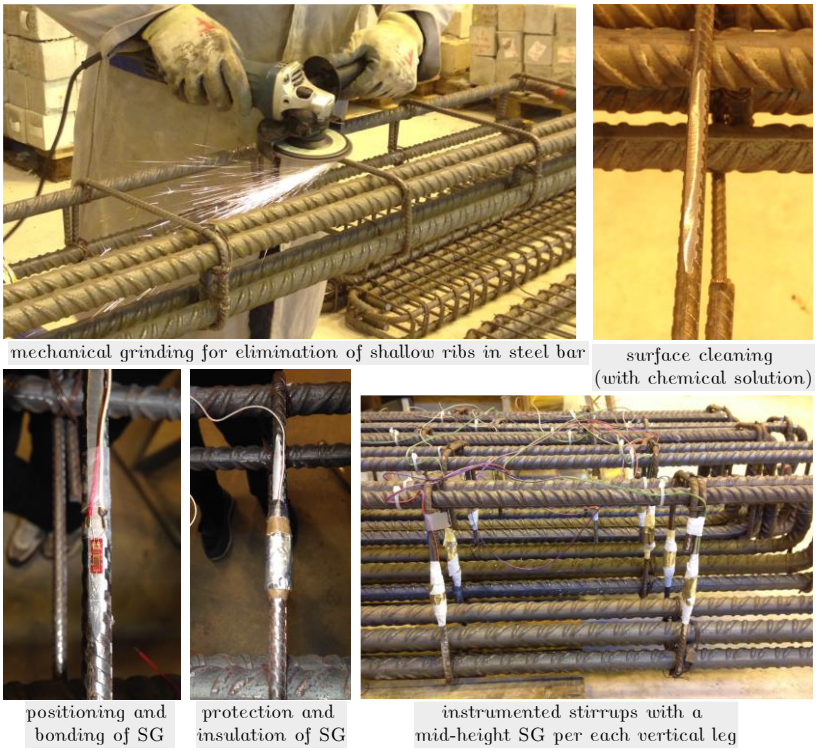

Figure 5: Instrumentations of steel stirrups with electrical strain gauges.

The beams are cast using a batch of normal-weight concrete with target (characteristic cubic) compressive strength of 25 MPa (C20/25 grade), using ordinary Portland cement (32.5 R) with slump S3, as verified during the casting phase in compliance with UNI EN 12350-2, and maximum aggregate size of 15 mm.

After casting, the fresh concrete is vibrated and mixed (to avoid segregation and bleeding) and then the beams are left in the formworks for 48 hours and covered with a cellophane sheet to prevent water evaporation and to control the curing process, after which they are demolded and left cured at environmental conditions (temperature 20±3 °C, relative humidity 65-75%) as shown in Figure 6. The average concrete compressive strength, determined within two weeks of the day of beam testing as average of three cubes (150 mm side) in accordance with UNI EN12390-3, is R_{cm} = 36.1 MPa (CoV 0.056), while the average concrete flexural strength, determined as average of three prisms (150 x 150 x 600 mm) in accordance with UNI EN12390-5, is f_{fm} = 4.6 MPa (CoV 0.037).

A PBO-FRCM composite is used for strengthening the beams, realized with a bidirectional unbalanced open-mesh textile having commercial name PBO mesh gold 70/18 [30] (see Figure 7) combined with a cement-based (inorganic) matrix with designation MX-PBO [31]. The PBO mesh is composed of bundles (yarns) that are 5 mm wide in the warp direction (spaced

at 10 mm) and 2.5 mm wide in the weft direction (spaced at 17.5 mm) [27]. The equivalent thickness in the warp and weft direction, reported in the manufacturer's datasheet, is 0.045 mm and 0.012 mm, respectively.

Figure 6: Concrete casting and curing process of beams.

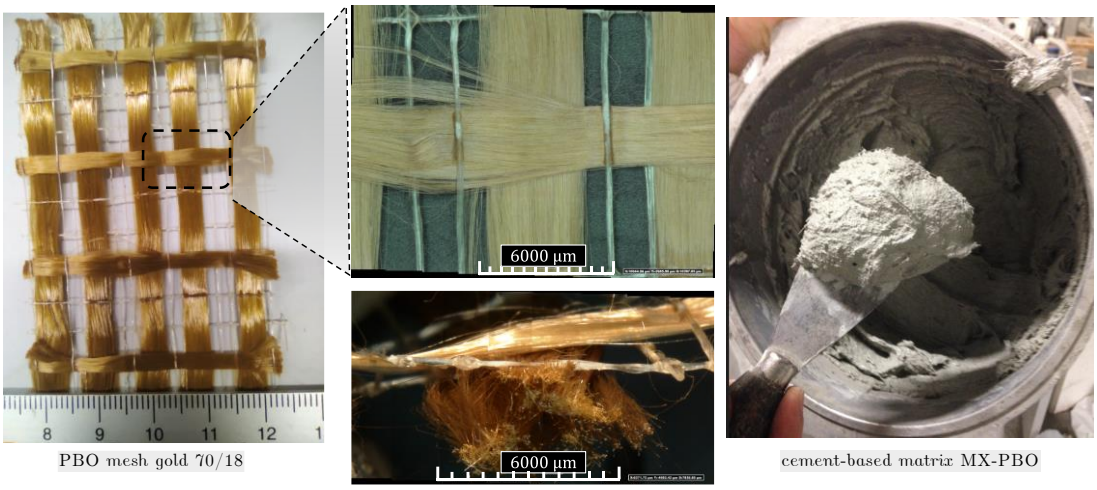

Figure 7: PBO-FRCM composite used for beam strengthening (numbers in ruler of left-side photo are in [cm]).

The PBO dry mesh has been tested to determine the tensile properties. Portion of the PBO mesh composed of 1, 2 and 5 bundles are cut from the 100 cm wide roll and tested up to failure (Figure 8). Tensile tests on the 5-bundle mesh are performed by means of a universal testing machine Zwick Roell Z600 (equipped with a 600 kN load cell), equipped with a sensor arm extensometer (accuracy class 0.5), while tensile tests on the 1-bundle and 2-bundle mesh are performed with an electric universal testing machine mod. Instron ElectroPuls E3000

(equipped with a 5 kN load cell). The mean values of tensile strength σ_{fu}, corresponding ultimate strain (at peak tensile strength) ε_{fu} and the elastic modulus E_f (calculated as a linear regression between points at axial strain ε_f =0.25% and ε_f =0.50%) are 1314 MPa, 1.96% and 85.3 GPa, respectively (CoV 0.23, 0.17, 0.48, respectively). It is worth noting that such values are systematically lower than those reported in the manufacturer's datasheets (σ_{fu} = 5800 MPa, ε_{fu} = 2.5% and E_f = 241 GPa); moreover, other authors reported higher mechanical properties for the same PBO mesh, e.g., D'Antino & Poggi (σ_{fu} = 4700 MPa, ε_f = 1.82% and E_f = 273 GPa) and Bertolesi et al. (σ_{fu} = 3905 MPa and E_f = 215.9 GPa). The marked differences might be ascribed to the storage conditions of the mesh before the tensile testing (the mesh was left in laboratory for around 2 years with relative humidity conditions variable between 65% and 75%). Further investigation from a microscopic/chemical viewpoint is underway to identify the causes of such mechanical degradation.

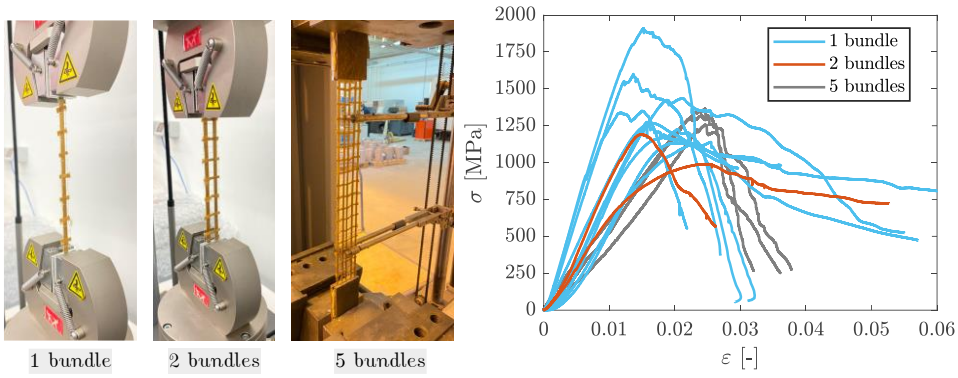

Figure 8: Tensile tests on dry PBO mesh composed of 1, 2 and 5 bundles.

Figure 9: Flexural and compressive tests on cement-based mortar used as matrix in the PBO-FRCM system.

To obtain the mechanical characteristics of the cement-based matrix, four 40x40x160 mm prisms are prepared the same day of the beam strengthening, cast in metallic formworks, covered by a wet cloth for 48 hours, then demolded and tested within two weeks of the day of beam testing. The average matrix flexural strength, determined in accordance with EN12390-5, is f_{fm} = 6.2 MPa (CoV 0.042), while the average matrix compressive strength, determined in accordance with UNI EN 196-1 on halves of the broken prisms, is R_{cm} = 40.8 MPa (CoV 0.131). The compressive strength of the cement-based mortar is also determined on three cubes having 50 mm side, in accordance with ASTM C-109: the average value is R_{cm} = 34.8 MPa (CoV 0.104).

2.3 Strengthening procedure

The beams are strengthened using a U-wrapped configuration scheme, continuous along the studied shear span as depicted in Figure 2. As a preliminary step, the position of stirrups along the studied shear span is identified through a rebar locator (pachometer), see Figure 10.

Before applying the PBO-FRCM system, the concrete surfaces are prepared via a preliminary sandblasting and rounding procedure (radius of approximately 20 mm at the two corners of the bottom face of the beam) so as to increase the grip of the bonded face and to avoid stress concentration at the corners of the cross section where the wrap direction changes suddenly.

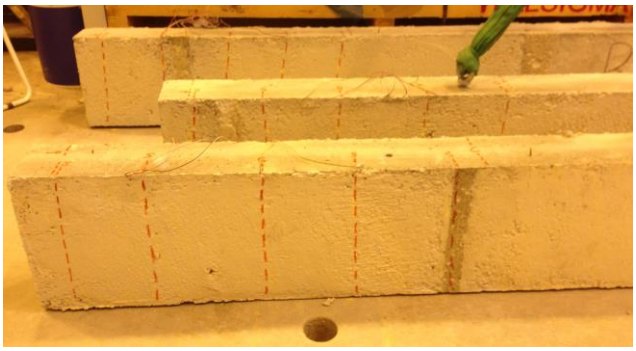

Figure 10: Identification of stirrups position through a rebar locator (pachometer).

Figure 11: Preparation of concrete surfaces where to apply the FRCM system.

It is worth noting that the PBO dry mesh is cut from the roll provided by the manufacturer (100 cm wide and 15 m long) in pieces having 300 mm width and 750 mm length. Three sheets of the PBO mesh having such dimensions are placed one besides the other (without overlapping) to cover the strengthening area of 900 mm in the U-wrapped configuration shown Figure 2. The fibers are instrumented with electrical strain gauges (gauge length 6 mm as those used for monitoring steel stirrups) attached in the same positions as those mounted in the stirrups for the beam type A and B (see again Figure 2). Such SGs are applied (bonded) directly onto the fiber bundles (wrap direction) and insulated through a special coating (commercial name "HBM protective ABM 75", a 0.05 mm thick aluminum foil coated with a 3 mm thick kneadable putty). Four and six SGs for the PBO mesh installed in beam type A and B are used, respectively, having nomenclature $SF_{i,front}$, $SF_{i,rear}$, as depicted in Figure 2.

The application of the externally bonded PBO-FRCM system entails the following steps, illustrated in Figure 12: i) wetting of the strengthening surfaces; ii) application of the first layer of mortar (thickness around 4 mm); iii) application of PBO mesh, which is first placed in

the appropriate position, tensioned and bonded onto the underlying fresh-state matrix through a slight pressure; iv) application of the second layer of mortar (thickness around 4mm), while the first layer is still fresh.

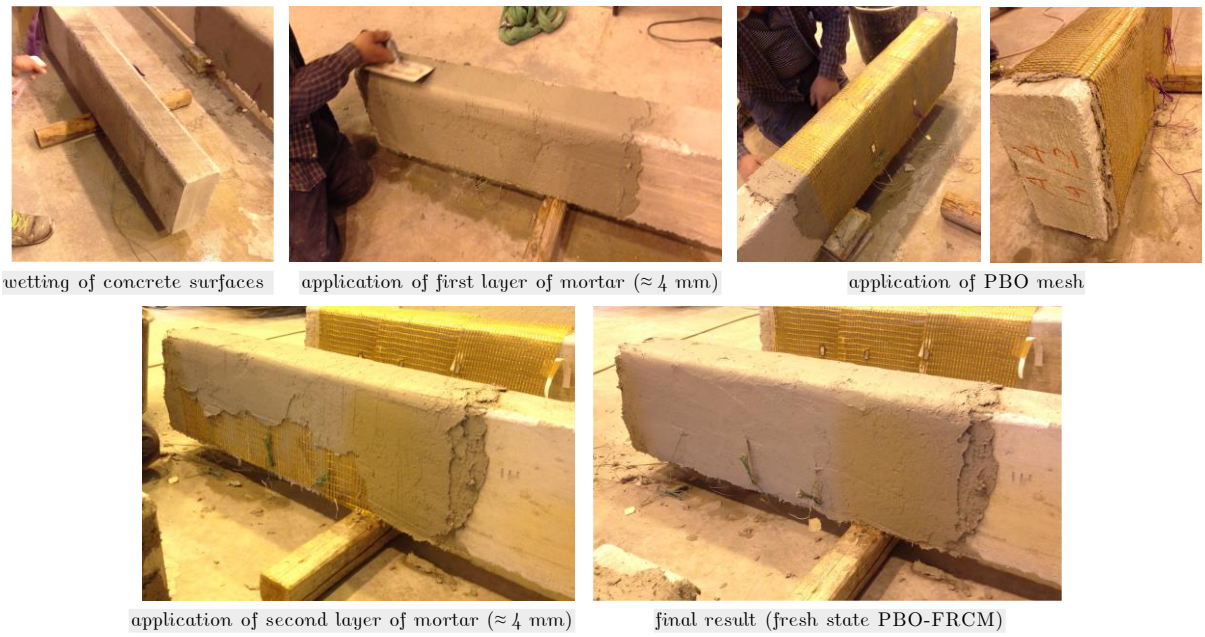

Figure 12: Strengthening procedures of beams through U-wrapped externally bonded PBO-FRCM system.

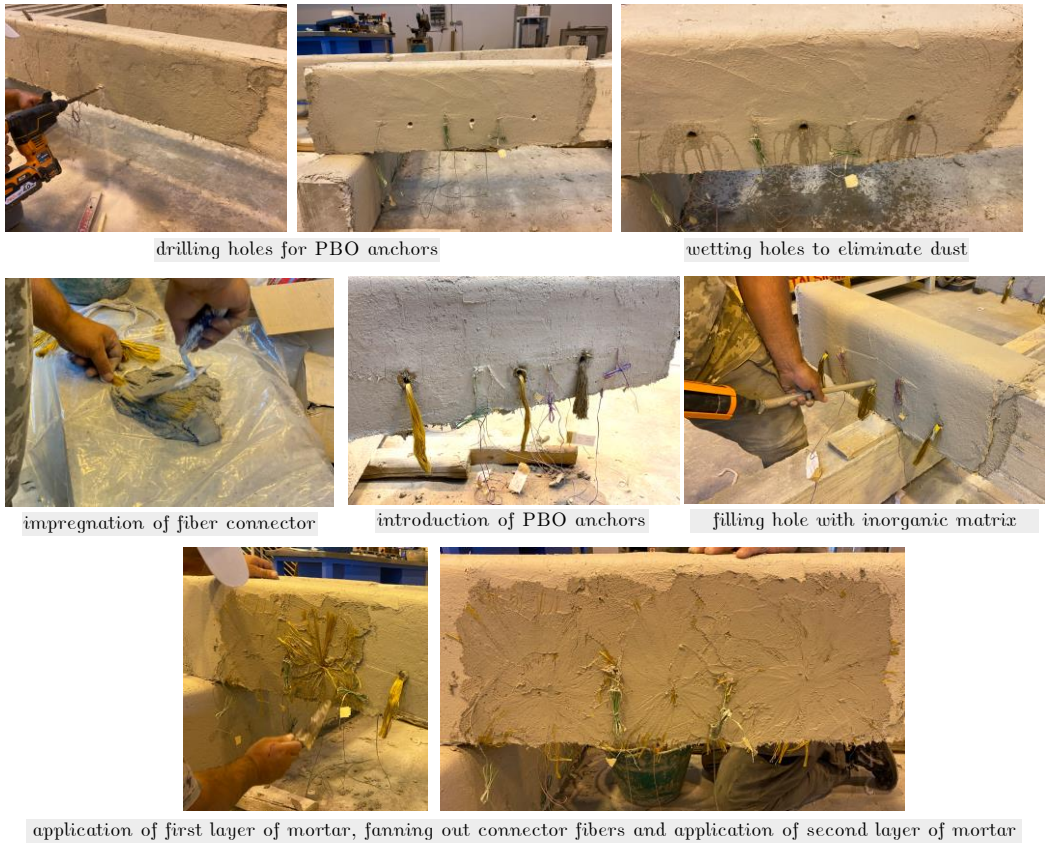

Figure 13: Sequence for the application of PBO fiber connectors (anchors).

In six of the eight shear strengthened beams, the FRCM jackets are anchored using fiber connectors with commercial name PBO-Joint [32], having 6 mm diameter and realized with unidirectional PBO fibers (tensile strength ≥ 1500 MPa, according to the manufacturer's datasheet). The anchors are installed 15 days after the above-described shear strengthening operations, to make sure that the FRCM system has completely hardened. The sequence of application of the PBO anchors is illustrated in Figure 13: *a*) first, holes with diameter 16 mm are drilled on the concrete faces, taking into careful consideration the position of stirrups (previously identified through the rebar locator); *b*) dust and impurities are eliminated with compressed air and holes are wetted; *c*) the PBO joint fiber connector is suitably cut at the desired length, equal to the 350 mm considering the width of the beam (150 mm) plus two additional segments of length around 100 mm that will be spread out from the two sides as described in the following phase *f*); *d*) one terminal of the joint is impregnated with MX-Joint inorganic matrix [33] and introduced into the hole; *e*) the connector is introduced in the hole and then the hole is filled with inorganic matrix (grout) applied through a specially designed piston tool; *f*) a first layer of cement-based mortar (approximately 4 mm) is applied all around the hole, then connector fibers are fanned out using a metal spatula and finally a second layer of mortar (approximately 4 mm) is applied to completely cover the anchor.

3 EXPERIMENTAL RESULTS

The main results of the testing campaign are listed in Table 2 in terms of maximum load (P_{max}), maximum shear (V_{max} = 0.5 P_{max}), shear provided by the strengthening system (V_f) computed as the maximum shear of the strengthened beam minus the maximum shear of the corresponding control specimen, percent increase in maximum shear over the control beam for the strengthened specimens (ΔV), displacement at mid-span corresponding to the maximum load (δ_{Pmax}), which represents a measure of the deformation capacity of the tested RC beams, and percent increase of deformation capacity over the control beam for the strengthened specimens (Δ_δ).

Table 2: Summary of test results.

Series	Beam	P_{max} [kN]	V_{max} [kN]	V_f [kN]	ΔV [%]	δ_{Pmax} [mm]	Δ_δ [%]
A	A-control	246.3	123.1	-	-	12.8	-
	A-1-90-a	299.4	149.7	26.5	21.6	16.3	27.8
	A-1-90-n	292.3	146.1	23.0	18.7	15.5	21.4
	A-2-90-a	318.6	159.3	36.2	29.4	15.8	23.7
	A-1-45-a	343.7	171.8	48.7	39.6	18.9	47.8
B	B-control	287.8	143.9	-	-	12.4	-
	B-1-90-a	339.5	169.7	25.8	18.0	18.4	44.0
	B-1-90-n	373.2	186.6	42.7	29.7	21.4	68.0
	B-2-90-a	362.1	181.0	37.2	25.8	19.8	55.3
	B-1-45-a	351.7	175.9	32.0	22.2	20.1	57.4

The results in Table 2 show that the use of U-wrapped PBO-FRCM system increases the shear strength relative to the control beams of variable amount, from around 20% to 40%, as well as increases the deformation capacity relative to the control beams of variable amount, from around 20% to more than 60%, depending on strengthening configuration. As expected, a generally higher increase of the strength and deformation capacity is obtained for the beams of series A (with lower amount of transverse reinforcement) than the beams of series B. Indeed, for the beams of series B (with stirrup spacing of 200 mm), a more pronounced interaction between the internal (steel stirrups) and external (FRCM sheets) shear reinforcement is

reasonably expected. The largest strength and ultimate deformation gain is obtained for the configuration with fibers oriented at 45° about the beam longitudinal axis in the beam A (specimen A-1-45-a).

With regard to the failure mode, the two control beams showed the typical shear failure with a main diagonal crack in the studied shear span from the loading point to the support plate, accompanied by secondary diagonal cracks forming close to the main crack (Figure 14).

Figure 14: Failure mode of control beams.

Similarly, all the FRCM strengthened beams exhibited a shear failure, with cracks visible on the surface of the FRCM jackets. In particular, cracks appear on the FRCM surface from early stages of loading (i.e., from loads of around 150 kN), and not only approaching the failure load. In general, the failure mechanism of strengthened beams (including those with or without anchors) includes a main diagonal crack crossing the shear span, starting close to the loading point up to the support region. Additionally, local detachment of the entire FRCM system close to the loading region, triggered by concrete crushing in the compressed zone, and subsequent fiber slippage along the diagonal crack are observed (Figure 15). The presence or not of the anchor did not modify this failure mechanism and did not prevent the local detachment, which was instead ascribed to the failure of the underlying concrete substrate (rather than to a delamination at the concrete-FRCM interface due to tangential stress). Moreover, the different orientation of the fibers, despite providing some differences in the resulting maximum shear, did not modify the failure mechanism in a marked manner.

With regard to the strain measurements obtained by the SGs, the largest fiber exploitation ratios (defined as $\varepsilon_{f,max}/\varepsilon_{fu}$, where $\varepsilon_{f,max}$ is the maximum fiber strain measured at the peak load) are observed in the second instrumented fiber and stirrup (i.e., ST_2 and SG_2), which fall close to the main diagonal crack. The fiber exploitation ratios vary between 18% (attained for beam A-2-90-a) and 39% (attained for beam B-1-45-a). Such values are in good agreement with results reported in another testing campaign by Gonzalez-Libreros et al. [14] for carbon and steel FRCM systems. On the other hand, the stirrups crossing the main diagonal crack are largely yielded. A measure of the post-elastic engagement of the steel stirrups is given by the $\varepsilon_{s,max}/\varepsilon_{sy}$ ratio (where $\varepsilon_{s,max}$ is the maximum steel strain measured at the peak load and ε_{sy} is the yielding strain calculated as f_{ym}/E_s, E_s = 200000 MPa being the elastic modulus of steel). The largest value of these steel engagement ratios are variable between 1.10 and 5.90, whereas in the control beam the ratios also reach values higher than 6. The presence of the anchorage did not modify the maximum shear significantly but had a marginal influence on the failure mode by preventing or just delaying the local detachment of the FRCM system from the concrete substrate.

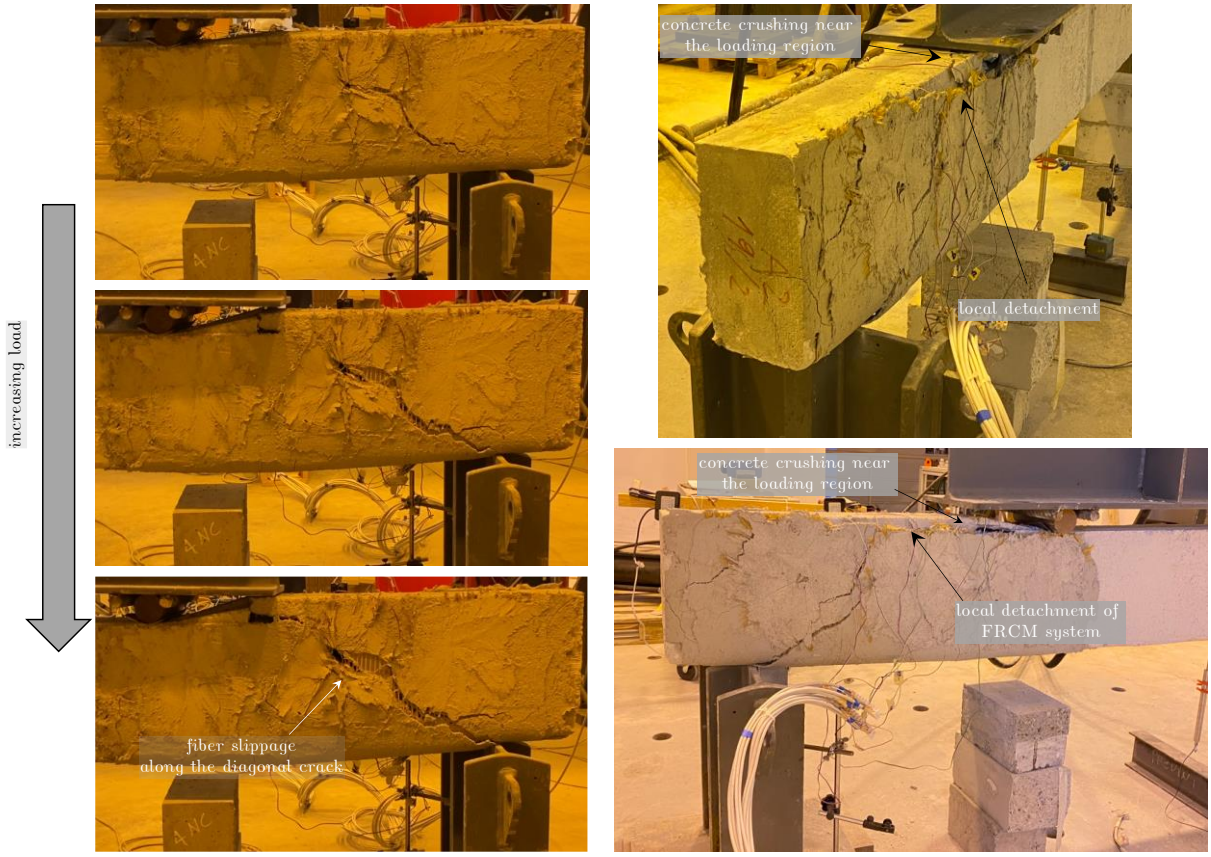

Figure 15: Failure mode of A-1-90-a beam.

4 NUMERICAL SIMULATION

A numerical model of the RC beams (with and without FRCM) is carried out with the 3D finite element code ATENA [34], in order to test the capability to simulate the experimental behavior of the specimens. The numerical model is based on a fracture-plastic approach for concrete material, termed "*CC3DNonLinCementitious2*", combining tensile fracture behavior and compressive plastic behavior. In particular, a smeared crack approach based on Rankine criterion is adopted for describing the tensile response of concrete, whereas concrete crushing

is modelled via a 3D Menétrey-Willam failure surface [35] with hardening plasticity. Concrete material parameters assigned in the model are consistent with experimental findings; nonlinear material parameters that were not determined in the experimental campaign, such as fracture energy, tension stiffening parameters and shear retention factors, are set based on conventional assumptions for ordinary concretes, consistent with the mechanical properties of related compressive and tensile strength values identified from the tests.

Ordinary reinforcing steel bars (longitudinal and transverse) are modeled in their exact locations through discrete embedded truss elements with a multilinear elastic-plastic material "*CCReinforcement*" calibrated upon the stress-strain experimental results.

The vertical load transferred from the actuator to the tested beam is distributed over two steel plates (linear elastic material "*CC3DElastIsotropic*"), while another couple of steel plates simulate the effect of the supports (all having 0.06 m width) with zero imposed displacement in the *z* direction. Master-slave constraints are adopted at each concrete-plate pair.

The FRCM system is simulated through 3D solid elements for the matrix, combined with embedded truss elements for the fibers, the latter incorporating an analytical bond-slip law ("*BarWithBond*"). In particular, the PBO fibers are modeled with equivalent rectangular cross section (based on the equivalent thickness of the fabric and the spacing of the rovings [27]), and bond-slip behavior at the fiber-matrix interface is simulated based on the analytical formulation proposed by Zou et al. [36] for the same PBO textile used in this experimental campaign. After a preliminary mesh sensitivity study, 8932 3D solid elements (consisting of 1705 tetrahedral elements and 7227 hexahedral elements) and 436 embedded truss elements are used – see Figure 16. A nonlinear solver (PARDISO) with Newton-Raphson method is used to solve the governing nonlinear equations.

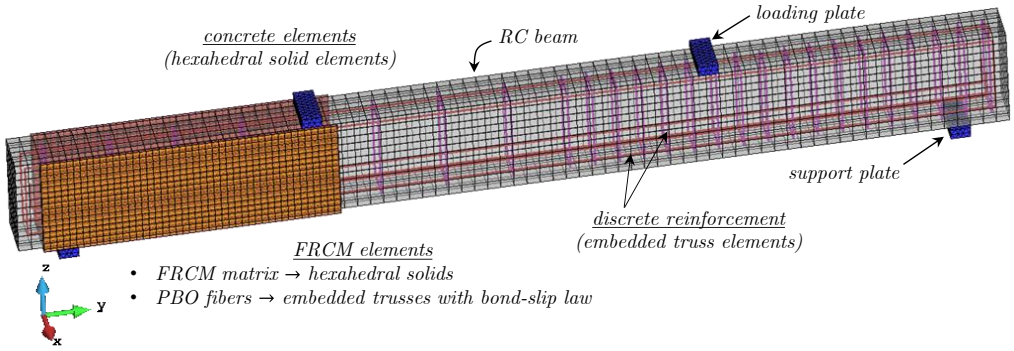

Figure 16: 3D nonlinear finite element (FE) model of the RC beam with FRCM system.

A multi-step nonlinear static analysis is carried out. After application of boundary conditions, the subsequent step incorporates a pushdown analysis with monotonically increasing load up to failure. At each step, the strain in the stirrups and fibers are monitored, along with the development of cracks and the load-displacement curve. In this contribution, only some representative results are shown for the sake of brevity. In particular, Figure 17 illustrates the crack at peak load of the bond slip vis-à-vis the experimental failure mode of the beam B-1-90-n that is simulated. The model is quite able to predict the diagonal crack arising from the loading point to the support region and is sufficiently accurate in describing the load-displacement response of the tested beam. Further refinements are, of course, possible by slightly modifying the nonlinear parameters of concrete.

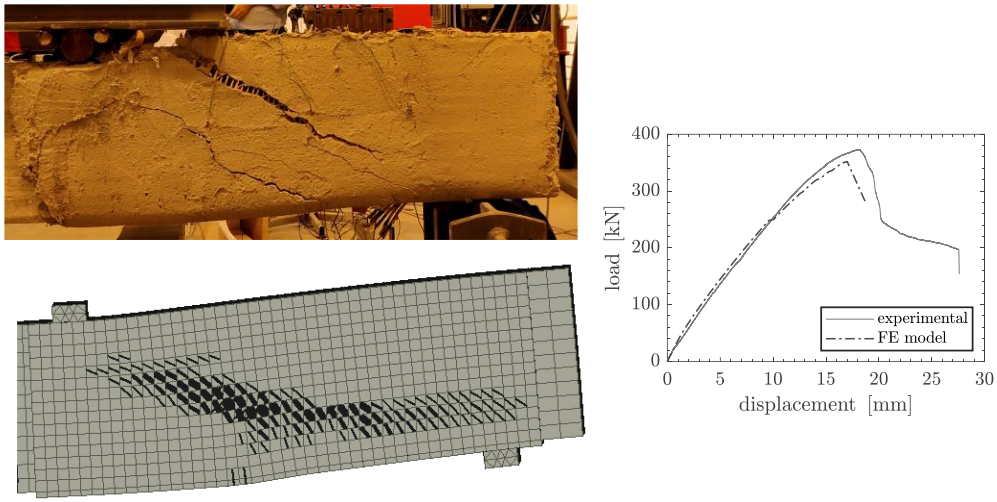

Figure 17: Numerical versus experimental results for the B-1-90-n beam.

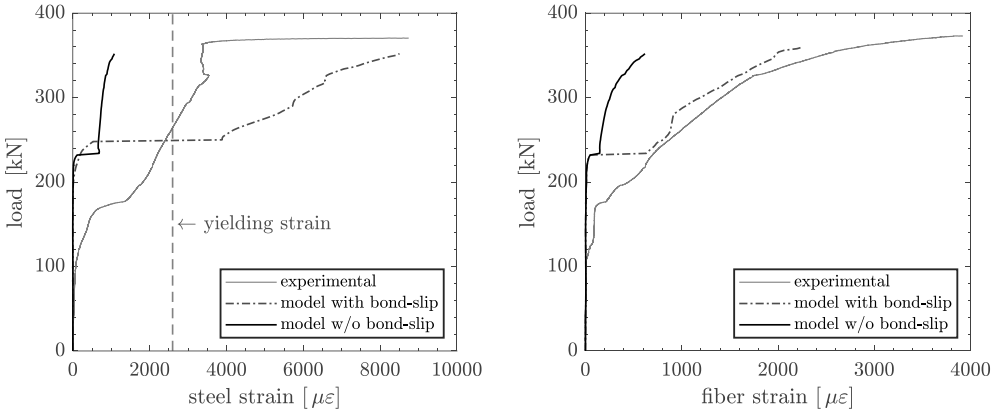

Figure 18: Numerical strains obtained in the FE model in the steel stirrups (left) and PBO fibers (right).

By looking at the local results crossing the diagonal crack in the B-1-90-n beam (fiber 2, stirrup 2, according to the nomenclature in Figure 1 and Figure 2), it is interesting to compare the numerical strain values obtained in the FE model with those obtained from the SGs in the experimental tests, see Figure 18. We point out that the measurements with the SGs might be affected by local phenomena (e.g., contact with aggregates during casting, local fracture in the region surrounding the bonding point, etc.) that cannot be simulated in the FE model. However, the order of magnitude of the strains numerically obtained is in good agreement with the experimental findings. As an example, the model predicts that the mid-height of the stirrup 2 has locally exceeded the yielding strain at a load roughly equal to 250 kN, which is in good agreement with the experimental findings.

The order of magnitude of the fiber strains is also reasonably consistent with the experimental results (values at peak load equal to 2000 με, corresponding to a fiber exploitation ratio of around 10% in this case). On the other hand, a numerical model that neglects the bond-slip behavior at the fiber-matrix interface would lead to poorer predictions of the strains and of the associated failure mode: in general, lower values of steel and fiber strains would be obtained by such a model, as reported in the plots of Figure 18.

Further refinements of the numerical simulation could imply the addition of an interface element in between the FRCM matrix and the concrete substrate, in order to simulate possible

local detachments observed in some of the tested beams, besides the fiber slippage phenomena within the FRCM composite that are already incorporated in this model.

5 CONCLUSIONS

In this contribution, we have presented the results of an experimental campaign focused on the shear strengthening of RC beams through U-wrapped externally bonded PBO-FRCM systems. Different variables have been investigated in the tests, including the fiber orientation (90° and 45° with respect to the beam longitudinal axis), the number of layers (one and two), the stirrup spacing (200 and 300 mm), and the presence or not of the anchorage.

All the strengthened beams tested in this study have failed in shear, with a main diagonal crack crossing the shear span, from the loading point up to the support region. Furthermore, local detachment of the FRCM system near the loading region accompanied by subsequent fiber slippage has also been noted, which is triggered by concrete crushing in the compressed zone. The results have shown that the shear strength gain contributed by the FRCM is more pronounced in the beams with larger stirrup spacing (i.e., lower transverse reinforcement ratios), as reasonably expected. The largest shear strength gain (39.6%) has been obtained in the beam with stirrup spacing equal to 300 mm and fibers oriented at 45°. This strengthening configuration, not widely investigated in the literature, seems quite promising and deserves further investigation in subsequent studies.

Although the presence of anchors has slightly modified the failure mode and the crack widths at peak load, the influence on the shear strength has been found to be marginal. It has been found that fiber exploitation ratios are variable in the range 18%-39% and are reasonably consistent with values reported in the literature for other FRCM systems (with alternative carbon and steel fabrics).

Preliminary numerical simulation with a nonlinear 3D FE model has also been carried out to study some local mechanisms and to establish a validated model for a more systematic analysis of the internal-external shear reinforcement interaction through combined experimental-numerical approaches.

ACKNOWLEDGMENTS

This research was funded by the P.O. FESR Sicilia 2014/2020 (Axis 1, Action 1.l.5 “Support for the technological advancement of companies through the financing of pilot lines and actions for early validation of products and large-scale demonstrations”) Project 082030000276 SMART-ART “Sviluppo di metodi avanzati di restauro, diagnostica e telecontrollo per la conservazione del patrimonio artistico architettonico”, CUP G79J18000620007.

REFERENCES

[1] Masi, A., & Vona, M. (2012). Vulnerability assessment of gravity-load designed RC buildings: Evaluation of seismic capacity through non-linear dynamic analyses. *Engineering Structures*, *45*, 257-269.

[2] Masi, A. (2003). Seismic vulnerability assessment of gravity load designed R/C frames. *Bulletin of Earthquake Engineering*, *1*, 371-395.

[3] Magenes, G., & Pampanin, S. (2004). Seismic Response of Gravity-Load Design Frame with Masonry Infills. *13th World Conf. Earthq. Eng.,* Vancouver, Canada.

[4] Calvi, G., & Pampanin, G. (2002). Experimental test on a three storey RC frame designed for gravity only, *12th European Conf. Earthq. Eng.,* London, UK, Paper 727.

[5] Italian Ministry of Infrastructures and Transportations (2018) NTC2018. Aggiornamento delle «Norme tecniche per le costruzioni». Decreto 17 Gennaio 2018, Supplemento ordinario alla Gazzetta ufficiale n. 42, 20 February 2018 (In Italian).

[6] European Committee for Standardization. Eurocode 8: design of structures for earthquake resistance—part 1: general rules, seismic actions and rules for buildings. EN 1998-1:2004+A1: 2013. Brussels, Belgium; 2004.

[7] ASCE/SEI Standard 41–17. Seismic evaluation and retrofit of existing buildings. American Society of Civil Engineers, Reston, Virginia, USA; 2017.

[8] SEAOC (1995). "Performance-based seismic engineering." in. Vision 2000 committee. Sacramento, CA: Structural Engineers Association of California.

[9] ASCE (2000). FEMA 356 – prestandard and Commentary for the seismic rehabilitation of buildings. Reston, VA: ASCE-American Society of Civil Engineers.

[10] ACI Committee 549 *ACI 549.6R-20 Guide to Design and Construction of Externally Bonded Fabric-Reinforced Cementitious Matrix* 587 *(FRCM) and Steel-Reinforced Grout (SRG) Systems for Repair and Strengthening Masonry Structures*; 2020.

[11] Carozzi, F. G., Bellini, A., D'Antino, T., de Felice, G., Focacci, F., Hojdys, Ł., ... & Poggi, C. (2017). Experimental investigation of tensile and bond properties of Carbon-FRCM composites for strengthening masonry elements. *Composites Part B: Engineering*, *128*, 100-119.

[12] De Domenico, D., Fuschi, P., Pardo, S., & Pisano, A. A. (2014). Strengthening of steel-reinforced concrete structural elements by externally bonded FRP sheets and evaluation of their load carrying capacity. *Composite Structures*, *118*, 377-384.

[13] De Felice, G., Aiello, M. A., Caggegi, C., Ceroni, F., De Santis, S., Garbin, E., ... & Viskovic, A. (2018). Recommendation of RILEM Technical Committee 250-CSM: Test method for Textile Reinforced Mortar to substrate bond characterization. *Materials and Structures*, *51*, 1-9.

[14] Gonzalez-Libreros, J. H., Sneed, L. H., D'Antino, T., & Pellegrino, C. (2017). Behavior of RC beams strengthened in shear with FRP and FRCM composites. *Engineering Structures*, *150*, 830-842.

[15] Marcinczak, D., Trapko, T., & Musiał, M. (2019). Shear strengthening of reinforced concrete beams with PBO-FRCM composites with anchorage. *Composites Part B: Engineering*, *158*, 149-161.

[16] D'Antino, T., Focacci, F., Sneed, L. H., & Pellegrino, C. (2020). Shear strength model for RC beams with U-wrapped FRCM composites. *Journal of Composites for Construction*, *24*(1), 04019057.

[17] Faleschini, F., Zanini, M. A., Hofer, L., Toska, K., De Domenico, D., & Pellegrino, C. (2020). Confinement of reinforced concrete columns with glass fiber reinforced cementitious matrix jackets. *Engineering Structures*, *218*, 110847.

[18] Ombres, L. (2014). Concrete confinement with a cement based high strength composite material. *Composite Structures*, *109*, 294-304.

[19] Raoof, S. M., Koutas, L. N., & Bournas, D. A. (2017). Textile-reinforced mortar (TRM) versus fibre-reinforced polymers (FRP) in flexural strengthening of RC beams. *Construction and Building Materials*, *151*, 279-291.

[20] De Domenico, D. (2015). RC members strengthened with externally bonded FRP plates: A FE-based limit analysis approach. *Composites Part B: Engineering*, *71*, 159-174.

[21] Bencardino, F., Carloni, C., Condello, A., Focacci, F., Napoli, A., & Realfonzo, R. (2018). Flexural behaviour of RC members strengthened with FRCM: State-of-the-art and predictive formulas. *Composites Part B: Engineering*, *148*, 132-148.

[22] Colombi, P., & D'Antino, T. (2019). Analytical assessment of the stress-transfer mechanism in FRCM composites. *Composite Structures*, *220*, 961-970.

[23] Sneed, L. H., D'Antino, T. O. M. M. A. S. O., Carloni, C., & Pellegrino, C. (2015). A comparison of the bond behavior of PBO-FRCM composites determined by double-lap and single-lap shear tests. *Cement and Concrete Composites*, *64*, 37-48.

[24] De Domenico, D., Urso, S., Borsellino, C., Spinella, N., & Recupero, A. (2020). Bond behavior and ultimate capacity of notched concrete beams with externally-bonded FRP and PBO-FRCM systems under different environmental conditions. *Construction and Building Materials*, *265*, 121208.

[25] De Domenico, D., Quattrocchi, A., Alizzio, D., Montanini, R., Urso, S., Ricciardi, G., & Recupero, A. (2021). Experimental characterization of the FRCM-concrete interface bond behavior assisted by digital image correlation. *Sensors*, *21*(4), 1154.

[26] Bertolesi, E., Carozzi, F. G., Milani, G., & Poggi, C. (2014). Numerical modeling of Fabric Reinforce Cementitious Matrix composites (FRCM) in tension. *Construction and Building Materials*, *70*, 531-548.

[27] D'Antino, T., & Poggi, C. (2021). Characterization and design of multilayer PBO FRCM composite reinforcements for concrete structures. *Journal of Composites for Construction*, *25*(6), 04021048.

[28] Focacci, F., D'Antino, T., & Carloni, C. (2020). The role of the fiber–matrix interfacial properties on the tensile behavior of FRCM coupons. *Construction and Building Materials*, *265*, 120263.

[29] De Domenico, D., Maugeri, N., Longo, P., Ricciardi, G., Gullì, G., & Calabrese, L. (2022). Clevis-Grip Tensile Tests on Basalt, Carbon and Steel FRCM Systems Realized with Customized Cement-Based Matrices. *Journal of Composites Science*, *6*(9), 275.

[30] Ruregold srl. 2019. "Technical datasheet of PBO-Mesh 70/18." Accessed March 11, 2023. https://ruregold.com/download/pbo-mesh-70-18-data-sheet.

[31] Ruregold srl. 2021. "Technical datasheet of MX-PBO concrete." Accessed March 11, 2023. https://ruregold.com/download/mx-pbo-concrete-data-sheet.

[32] Ruregold srl. 2019. "Technical datasheet of PBO-Joint." Accessed March 11, 2023. https://ruregold.com/download/pbo-joint-data-sheet/.

[33] Ruregold srl. 2021. "Technical datasheet of MX-Joint." Accessed March 11, 2023. https://ruregold.com/download/mx-joint-data-sheet.

[34] Červenka, V., Jendele, L., Červenka, J. 2020. "ATENA Program Documentation Part 1 Theory". Červenka Consulting: Prague, Czech Republic, 2020.

[35] Menétrey P, Willam KJ. A triaxial failure criterion for concrete and its generalization. ACI Struct J 1995;92:311–8.

[36] Zou, X., Sneed, L. H., D'Antino, T., & Carloni, C. (2019). Analytical bond-slip model for fiber-reinforced cementitious matrix-concrete joints based on strain measurements. *Journal of Materials in Civil Engineering*, *31*(11), 04019247.